Discovery of a Large-scale Porphyry Molybdenum Deposit in Tibet through a Modified TEM Exploration Method

Guo-Qiang Xue[1], Ke-Zhang Qin[1], Xiu Li[2], Guang-Ming Li[1], Zhi-Peng Qi[2] and Nan-Nan Zhou[1]
[1]Key Laboratory of Mineral Resources, Institute of Geology and Geophysics, Chinese Academy of Sciences, Beijing, 100029, China
Email: ppxueguoqiang@163.com, qqxueguoqiang@hotmail.com
[2]College of Geology Engineering and Geomatics, Chang'an University, Xi'an, 710054, China
Email: lixiu@chd.edu.cn

ABSTRACT

During the last decade, there have been many exploration achievements in the Tibetan Gangdese metallogenic belt. The Sharang area of the Tibetan region is covered by a low-temperature mineralized alterable clay that is considered to be a low-grade ore. Although small intervals of rich molybdenum (Mo) mineralization have been discovered, the ore deposit scale is limited and the condition of deep ore is still unknown. To explore these deeper targets, a modified large-loop TEM system was used in the Sharang area. The TEM receiver configuration is redesigned and the late-time resistivity equation of large-loop TEM has also been defined. During data processing, two regions with low resistivity anomalies were discovered. The interpreted results indicate that the main ore deposit is buried 200 m beneath the surface, and extends 600 m vertically. The total anomalous area associated with the ore deposit is estimated at 3.77 km^2. The interpretation results are consistent with drilling data acquired after the geophysical survey. The results show that it is the first ultra-large porphyry molybdenum deposit that has been found in Tibet.

Introduction to the Discovery and Mining Area

In recent years, much resource assessment and geological research has been carried out in Tibet, China. Preliminary results suggest enormous potential resources of porphyry deposits in the Gangdese metallogenic belt (Li and Rui, 2004; Li *et al.,* 2006; Qin, 2008; Zhao *et al.,* 2009), including a series of large porphyry Cu (Mo) deposits (Li *et al.,* 2007; Xiao *et al.,* 2008, 2009) and a large porphyry-skarn copper (with lead and zinc) composite bed. The discovered deposit in the Gandese metallogenic belt is about 1,000-km in length from east to west (E-W) and 100-km in width from north to south (N-S). Prospecting for porphyries in the Gangdese metallogenic belt is attracting much attention.

The Sharang ore enrichment area of Tibet is located in the eastern Gangdese volcanic and igneous metallogenic belt, of which the mineralized surface was discovered by previous geological exploration. It has been considered by researchers that a molybdenum ore body might occur in the plagioclase granite porphyry, suggested by hydrothermal vein ore deposits with a general E-W trend. Therefore, the preliminary works focused on the delineation of hydrothermal vein-type ores controlled by fracture zones, but the overall resource was neglected, particularly the potential of the mineralized porphyry body.

In 2007, the Jinhua Mining Development Company of Tibet obtained permission for mineral exploration, and invited the Institute of Geology and Geophysics, Chinese Academy of Sciences, to direct the field research in the Sharang molybdenum deposit area, Gongbujiangda County, Tibet. After a preliminary investigation, it was determined that the presence of porphyry mineralization supported the need to assess the resource potential of the region. According to surveys and analyses of existing data, the most promising area is located in the Gangdese belt, which has favorable mining conditions. The surface of the area is covered with clay resulting from low-temperature mineralization (Fig. 1) with small, but rich veins of molybdenum exposed (Fig. 2). The scale of ore deposit is uncertain since its extent at depth is unknown.

Mineral resources are of vital importance to China's national economy, which has led to a great deal of emphasis on "second phase" exploration work (Teng, 2007; Teng, 2008), where geophysical research becomes more important and new geophysical technologies need

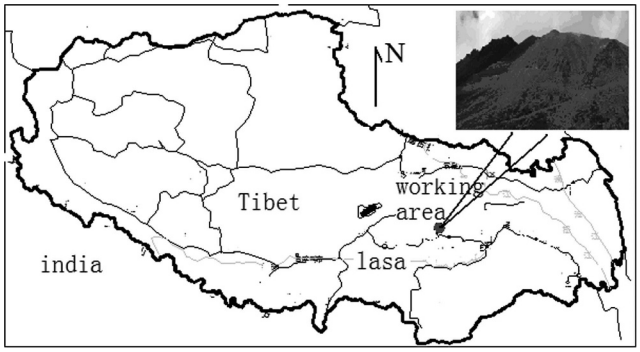

Figure 1. Surface mineralization and location of survey area (small figure at the right upper corner shows the mineralized altered surface of the survey area).

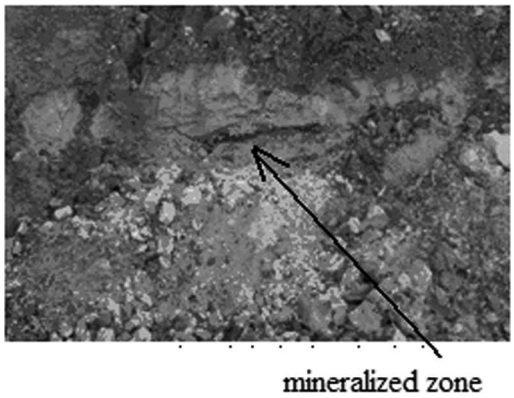

Figure 2. Exposed molybdenum ore at the surface (the arrow indicates the mineralized zone).

to be involved in deep geological exploration. The main purpose of this geophysical study is: 1) to determine the scope of abnormal mineralization within the range of 500-m underground, including the depth and extension of surface ore; 2) to determine the distribution of mineralization abnormalities in the main mineralized locations within a depth of about 700 m; and 3) to identify possible locations to drill verification holes.

A modified large-loop TEM technology was used for deep geological exploration in this study. The method involves: 1) exciting a square wave of current within a large square loop and energizing a primary field underground; 2) the primary field is turned off and a secondary magnetic field is induced in the subsurface conductive material as the secondary field diffuses down through the earth (Li, 2002; Xue *et al.,* 2008); and 3) measuring the secondary magnetic field within a certain range in the earth, which is received by a magnetic antenna. A transmit loop well coupled with a target body is characterized by large amplitude, large magnetic moment, uniform field, and slow decay, which is suitable for deep prospecting.

Theoretically, the distribution of the electromagnetic field in the central area of the transmit loop is not uniform (Raiche, 1987; Jiang, 1998; Xue *et al.,* 2007). However, the equations of central loop devices are often applied to data processing, which are simple and quick, but with less accurate results. In some cases, large errors are induced by using the equations of central loop devices to calculate a non-center field. Thus, it is necessary to calculate the response within the loop at an arbitrary point, as well as the apparent resistivity. In general, this method involves the following TEM techniques: 1) calculating the electromagnetic field response at an arbitrary location within the loop; 2) calculating the apparent resistivity related to the measurement locations within the loop for data processing; 3) measuring the TEM response using a large-area magnetic core receiver for deep signal collection; and 4) analyzing the TEM results to identify the low resistivity anomalies, which are associated with ore-grade mineralization deposits. A description of this process using TEM data acquired in the Sharang region is given below.

Modified TEM Method

Calculation of Apparent Resistivity

Under normal circumstances, the following central loop equation is used to calculate the apparent resistivity for large-loop TEM (Li, 2002):

$$\rho_\tau(t) = \frac{\mu_0}{4\pi t}\left(\frac{2\mu_0 Mq}{5tV(t)}\right)^{2/3}, \qquad (1)$$

where $\rho_\tau(t)$ is apparent resistivity, t is time, V(t) is the secondary induced voltage received by the receiving coil, M is the transmit magnetic moment, q is the receiving area, and μ_0 is the magnetic permeability of free space.

In a homogeneous half-space, the vertical magnetic field ($H_z(\omega)$) at the center of the loop is (Li, 2002):

$$H_z(\omega) = \frac{I_0}{K_1^2 a^3}[3-(3+3K_1 a+K_1^2 a^2)e^{-k_1 a}], \qquad (2)$$

where k_1 is the wave number, a is the radius of the transmit loop, I_0 is the transmitter current, ω is angular frequency, and σ is conductivity.

The vertical magnetic field at a non-central point in the loop is (Li, 2002):

$$H_z(\omega) = I_0 a\int_0^\infty \frac{\lambda Z^{(1)}}{Z^{(1)}+Z_0} J_1(\lambda a)J_0(\lambda r)d\lambda, \qquad (3)$$

where $\lambda Z^{(1)}/(Z^{(1)} + Z_0)$ is the integral kernel function, $J_1(\lambda a)$ and $J_0(\lambda r)$ are Bessel functions, and r is the offset. $Z^{(1)}$ is the wave impedances of a layered earth and $Z_0 = -\frac{i\omega\mu_0}{\lambda}$.

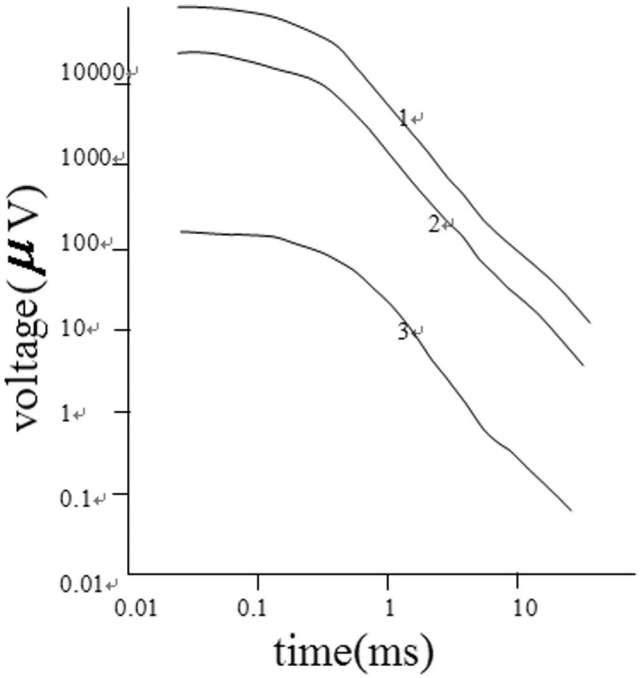

Figure 3. Decay curves of different antennas. In the figure, 1 indicates magnetic core probe (receiver area 40,000 m^2); 2 indicates magnetic probe (receiver area 10,000 m^2) and 3 indicates non-magnetic coil (receiver area 100 m^2).

Equation (3) is not easy to implement directly, but can be represented in a form similar to Eq. (2) (Qi, 2009):

$$H_z(\omega) = \frac{I_0}{k_1^2 a^3}\left[c_1 + \left(c_2 + c_3 k_1 a + c_4 k_1^2 a^2\right) e^{-k_1 a}\right], \quad (4)$$

where c_1, c_2, c_3, and c_4 are coefficients. These polynomial coefficients can be obtained by using a fitting algorithm based on the least squares technique (Qi, 2009).

The apparent resistivity at a non-central point can be expressed as:

$$\rho_z(t) = \frac{\mu_0}{\pi \cdot t}\left[\frac{c_z \pi I_0 \mu_0}{4t\mu \partial H_z(t)/\partial t}\right]^{2/3}, \quad (5)$$

where $c_z = c_3/8 - c_2/40 - c_4/2$.

Improvement of Receiver Design

The detection of deep targets, *i.e.,* 300–500 m, is a relevant application of the TEM method. During this work, a receiving magnetic probe was used instead of a receiving air-coil to enable a greater depth of detection. The magnetic probe has a greater effective area (physical dimension), opposed to the small-area receiver loop of the air-coil antenna. The receiving magnetic probe is not

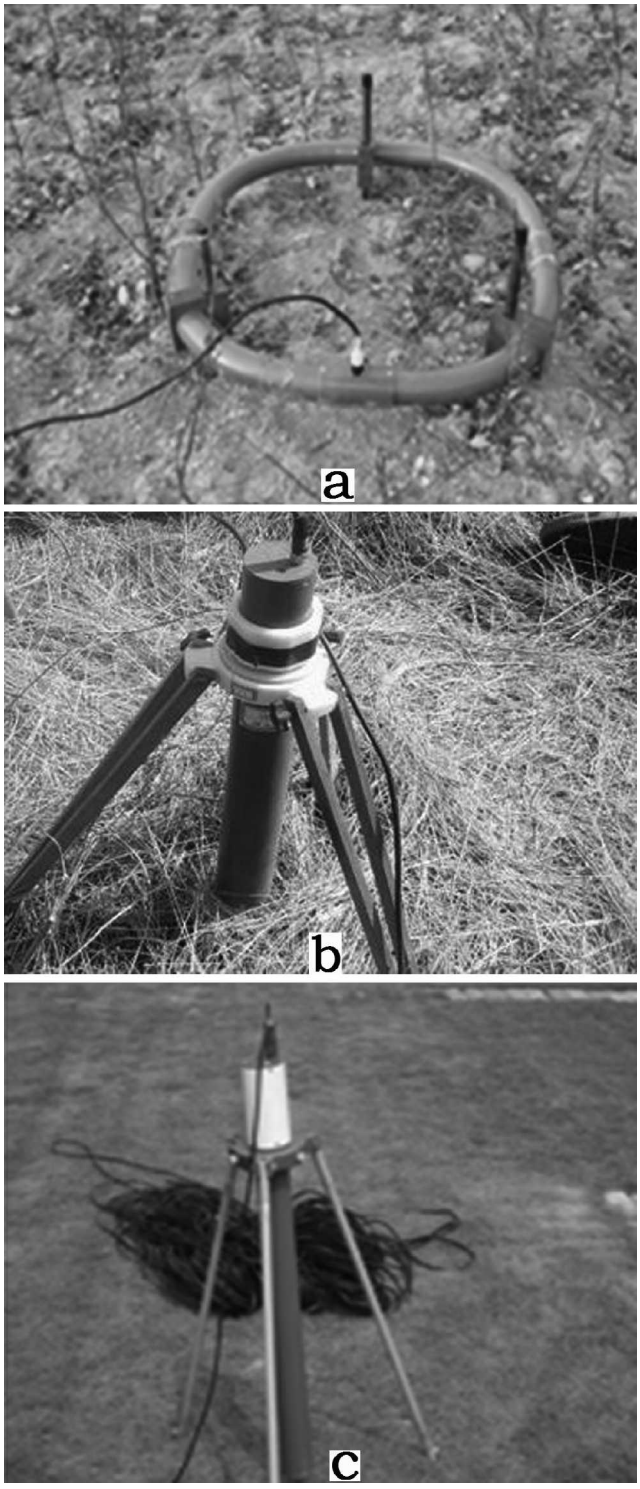

Figure 4. Receiver antennas: a) non-magnetic core coil (receiver area 100 m^2), b) magnetic core probe (receiver area 10,000 m^2), and c) magnetic core probe (receiver area 40,000 m^2).

Table 1. Comparison of different magnetic coils and the non-magnetic air coil.

Coil type	Optimum resonance	Amplitude (mV/nT)	Effective receiving area (m^2)
SB-7k	7.2k	1,288.69	40,000
SB-18k	17.1k	744.45	10,000
SB-70k	69.5k	570.61	2,000
SB-250k	245k	239.26	200
Air-coil	300k	118.75	100

only characterized by high sensitivity, good linearity, and large output dynamic range, but also is easy to level, the received signal is greatly improved, and the effective detection depth is increased.

In general, the lower the resonant frequency of the receiver coil, the longer the minimum sampling time will be, which leads to an increase in minimum and maximum depth of exploration (Ji *et al.,* 2007). The increased signal amplitude not only improves the signal-to-noise ratio, but also increases the time interval between useful signal and noise, leading to an increase in exploration depth. It is shown in Fig. 3 that receiver coils with different receiving areas (physical dimension) exhibit different decay curves under the same conditions. The larger the receiving area, the stronger the received signal will be. Benchmark tests indicate that the magnetic probe receives signals with larger amplitude and better results than that of the air-core coils. Therefore, the non-magnetic coil, specially designed for V8 (made by Phoenix Geophysics Ltd, Canada) with a smaller receiving area (Fig. 4(a)) was replaced by a magnetic probe that has a larger receiving area (Fig. 4(b)). Table 1 provides technical parameters of the magnetic probes and non-magnetic coil.

Application of Large Loop TEM in the Sharang Area

Prior to data collection, the resistivity of ore rock samples was measured (Table 2). It is clearly revealed that the resistivity of strong mineralized molybdenum ore is relatively low, leading to a measurable difference in electrical resistivity between an ore body and the surrounding rock. Thus, geophysical methods should be applicable for detecting the ore grade bodies.

Table 2. Results of stone sample measurements.

Sample no.	Averaged apparent resistivity (Ω-m)	Ore type
1	103	Weak mineralized molybdenum ore
2	99	Strong mineralized molybdenum ore
3	318	Surrounding ore

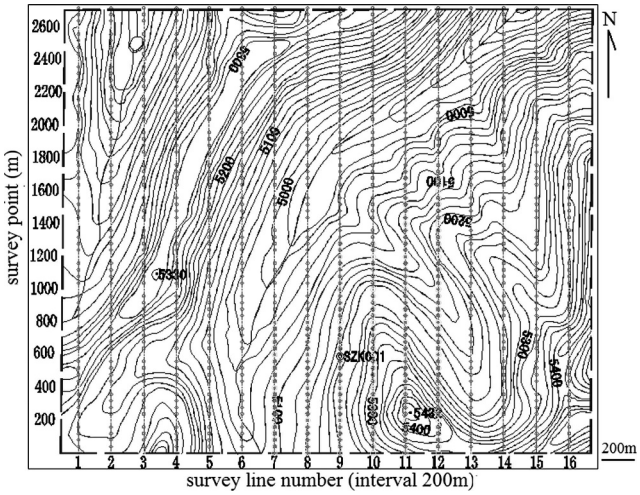

Figure 5. Sketch of survey lines (the grid size is 200 m × 40 m). Contours are topography.

The TEM equipment used is the Phoenix Geophysics V8 system with optional multi-function electrical instruments. System specifications include: transmitter coil 300 m × 300 m, 25 Hz and 8.3 Hz selected fundamental transmit frequencies with a total of 40 channels with time ranges of 0.072 ms to 8.64 ms and 0.216 ms to 25.92 ms, respectively. Equation (5) is used to calculate the apparent resistivity.

The survey area is a rectangular region about 3,100-m in length and 2,900-m in width (Fig. 5). The grid size is 200 m × 40 m, consisting of 1,168 survey points. The TEM data were interpreted to identify major anomalous areas for estimating ore volume and drilling locations to penetrate the ore bodies. Based on changes in apparent resistivity contours, the subsurface is divided into four layer units (Fig. 6). In profile from top to bottom, the range of apparent resistivity is: first (uppermost) unit 150–400 Ω-m, interpreted as the weathered surface layer; second unit 400–800 Ω-m, a moderately high resistivity layer of uneven thickness; third unit is mineralized within, 100–200 Ω-m, interpreted as low resistivity and presumed as porphyry with varying degrees of corrosion; and the fourth unit 250–400 Ω-m, interpreted as a moderately low resistivity body presumed as quartz sandstone and dolomite. In the apparent resistivity profile map, apparent resistivity contours with relatively low values (less than 200 Ω-m) are shown as a hatched area within an altitude of 4,500–5,000 m, which is interpreted as an abnormal body associated with mineralization.

To aid in understanding the difference between normal data and abnormal data, Table 3 gives the original induced voltage and calculated apparent resis-

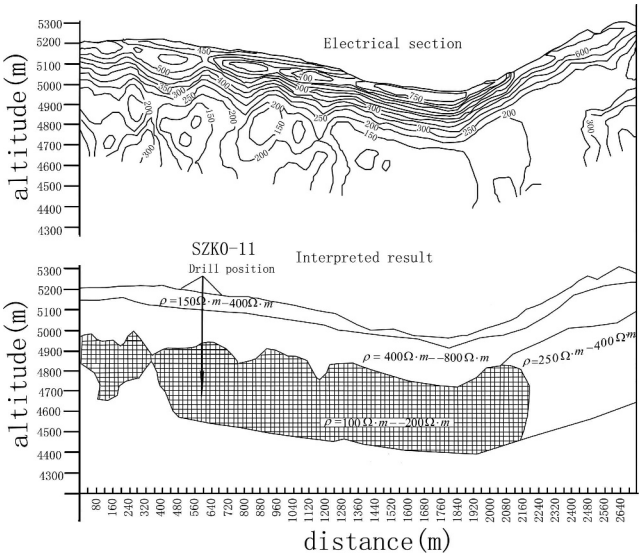

Figure 6. Cross-section based on integrated interpretation (the upper part is an apparent resistivity contour section, the lower part is the interpreted geologic section).

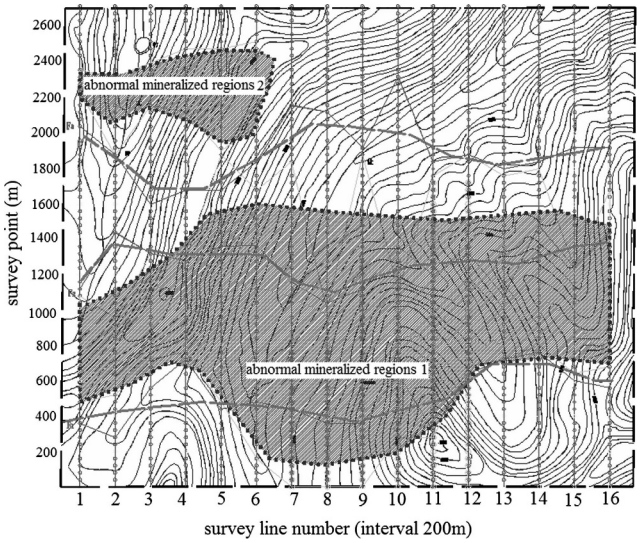

Figure 7. Plan view of both abnormal mineralized regions (the upper abnormal zone is named Region 2, the lower abnormal zone is named Region 1).

tivity of points 360 and 600, which are located in normal and abnormal positions, respectively, along the survey line (refer to Fig. 6). The induced voltage decays logarithmically in the later stage of the observation period, which corresponds to a gradual reduction in the calculated apparent resistivity values. The underground geologic structure can be deduced based on the characteristics of the decay curves.

The results of the TEM soundings indicate two anomalous zones related to mineralized regions within the survey area (Fig. 7). The larger one (region 1) crosses the survey area in an east-west direction with a length of about 3,000 m, a maximum width of 2,190 m, and

Table 3. Comparison of sounding data between a normal point (Point 360) and abnormal point (Point 600) along a typical line.

	Voltage (mV)	Voltage (mV)	Apparent resistivity (Ω-m)	Apparent resistivity (Ω-m)
Time (ms)	Point 360	Point 600	Point 360	Point 600
0.0010575	22.32	32.43	606.73	472.84
0.0011865	17.39	26.76	583.39	438.04
0.0013313	14.73	21.38	531.23	415.02
0.0014937	11.34	18.86	515.47	367.35
0.001676	8.76	15.80	498.84	336.82
0.0018805	8.42	13.53	417.88	304.74
0.0021099	7.15	11.21	379.38	281.19
0.0023673	5.75	9.75	357.34	251.47
0.0026562	4.90	7.37	324.13	247.10
0.0029803	4.32	5.99	287.91	231.47
0.003344	3.79	5.60	255.69	197.14
0.003752	3.54	4.38	217.23	189.14
0.0042098	3.47	4.20	180.22	158.61
0.0047235	2.84	3.62	169.88	142.66
0.0052998	1.99	2.93	163.30	133.82
0.0059465	1.73	3.05	155.63	106.12
0.0066721	1.28	2.47	153.17	99.72
0.0074862	0.95	2.08	153.91	91.06

Figure 8. Core from drill hole showing mineralization along a fracture (The pencil pit shows the molybdenum ore).

minimum width of 140 m. The maximum thickness of this anomaly is about 590 m, while the minimum is about 120 m. The mineralized anomalies have an elevation ranging from 4,700 to 5,000 m. The ground projection area of this anomaly is about 3.42 km^2. A smaller anomaly (region 2) is located in the northwest corner of the surveyed area. This anomalous region is about 1,100-m in length, and roughly 660-m in maximum width and 160-m in minimum width. The maximum thickness of the anomaly is about 640 m, while the minimum is about 210 m. The ground projection area of anomalous region 2 is about 0.352 km^2. The total area of anomalous regions 1 and 2 is 3.77 km^2.

In 2008, subsequent to the geophysical surveys, detailed investigations were carried out in parts of the anomalous areas by the Tibetan Bureau of Geology and Mineral Exploration. A total of 19 holes were drilled, of which the maximum drilling depth was 600 m and the total sum of the drilling depths is about 9,300 m, with mineralization found in every hole. The borehole surveys show that the granite porphyry mineralization consists of molybdenum in varying degrees. From the surface to the buried depth of 350 m, molybdenum content is greater than 0.01% (by volume), and high-grade ores (molybdenum content above 0.5%) exist locally (Fig. 8). Metallic minerals mainly consist of molybdenum, pyrite, minor amounts of limenite, and chalcopyrite, among others. Gangue minerals constitute 95% of the ore rock and include feldspar, quartz, and sericite. Mineralization porphyry is granite-porphyry, of which the metallogenic type is identified as an independent-type porphyry molybdenum.

Conclusions

A magnetic receiver, having a large effective area that improves the received signal amplitude, was used with a large-loop TEM system to enahance detection of deep targets in the range 200–500 m depth. The equation for calculating the modified apparent resistivity of the large-loop TEM source was redefined and used for data processing and interpretation.

Based on TEM results, low-resistivity anomalous areas were identified and suggest that the main ore body is located 200-m below the surface, and extends a vertical distance of over 600 m. The total anomalous area is estimated at 3.77 km^2, which was verified by drilling data.

It is significant to delineate the discovery of the Sharang porphyry molybdenum deposit. Tibetan geophysical prospecting in recent years has shown a great promise. This discovery is a major breakthrough in identifying the origin of porphyry molybdenum minerals.

Acknowledgments

This work was supported by the National Nature Science Foundation (41030750, 41174090) and the Knowledge Innovation Project of the Chinese Academy of Science (KZCX2-YW-Q04-07). Many thanks to Dr. J. Chen, who works at The Leibniz Institute of Marine Sciences at the University of Kiel in German, for improving the English. The authors extend their gratitude to the editor for her editorial suggestions.

References

Jiang, B.Y., 1998, A practical near-zone magnetic source transient electromagnetic exploration (in Chinese with English abstract): Geological Publishing House, Beijing, 52–53.

Ji, Y.J., Lin, J., and Wang, Z., 2007, Analysis and numerical removing of distortion in transient electromagnetic receiver device for shallow sounding: Progress in Geophysics (in Chinese with English abstract), **22**(1), 262–26.

Li, G.M., and Rui, Z.Y., 2004, Diagenetic and mineralizationages for porphyry copper deposits in the Gangdise metallogenic belt, southern Tibet: Tectonics Geotectonica and Metallogenia (in Chinese with English abstract), **28**(2), 165–170.

Li, G.M., Liu, B., She, H.Q., Feng, C.Y., and Qu, W.J., 2006, Early Himalayan mineralization on the southern margin of the Gangdise metallogenic belt, Tibet, China: Evidence from Re-Osages of the Chongmuda skarn-type Cu-Au deposit: Geological Bulletin of China (In Chinese with English abstract), **25**(12), 1482–1486.

Li, G.M., Qin, K.Z., Ding, K.S., Liu, T.B., Li, J.X., Wang, S.H., Jiang, S.Y., and Zhang, X.C., 2006, Geology, mineralogy Ar-Ar age and mineral assemblage of Eocene Skarn Cu-Au Mo deposits in the southeastern Gangdese arc, southern Tibet: Implications for deep exploration: Resource Geology, **56**, 197–217.

Li, J.X., Qin, K.Z., Li, G.M., and Yang, L.K., 2007, K-Ar and Ar-Arages of Nimu porphyry copper field in Central Gangdese: Constrain on magmatic-hydrothermal evolution and ore-forming setting: Acta Petrologica Sinica (in Chinese with English abstract), **23**(5), 953–966.

Li, X., 2002, The theory and application of transient electromagnetic sounding, Shaanxi Science Technology Press, Xi'an, China.

Qin, K.Z., 2008, Discovery of large-scale porphyry molybdenum deposit, the first single Mo deposit in Tibet and its significance: Geology in China, **35**(6), 1101–1112.

Qi, Z.P., 2009, Definition of apparent resistivity of vertical and horizontal component based on large rectangular loop source: Annual of the Chinese Geophysical Society 2009, 10, 10–14, Hefei, China: 677–678.

Raiche, A.P., 1987, Transient electromagnetic field computations for polygonal loops on layered earth: Geophysics, **52**(6), 785–793.

Teng, J.W., 2007, Deep discover ore, exploration and exploitation for metal mineral resources and its deep dynamical process of formation: Progress in Geophysics (in Chinese with English abstract), **22**(2), 317–334.

Teng, J.W., 2008, The core scientific problems and development direction for contemporary geophysical research: Progress in Geophysics (in Chinese with English abstract), **23**(3), 637–640.

Xiao, B., 2008, Magmatic intrusion center and mineralization center of Qulong porphyry Cu2Mo deposit in Tibet: Evidence from fissure veinlets and mineralization intensity: Mineral Deposits, **27**, 200–208.

Xiao, B., 2009, S-rich, highly-oxidized ore-bearing Magma in the Qulong giant porphyry-type Cu-Mo deposit in Southern Tibet — Evidence from magmatogenic anhydrite: Acta Geologica Sinica (in Chinese with English abstract), **83**(12), 1860–1868.

Xue, G.Q., 2007, Characters of response of large-loop transient electro-magnetic field: Oil Geophysical Prospecting (in Chinese with English abstract), **42**(5), 586–590.

Xue, G.Q., Li, X., and Di, Q.Y., 2008, Research progress in TEM forward modeling and inversion calculation: Progress in Geophysics (in Chinese with English abstract), **23**(4), 1165–1172.

Zhao, J.X., Qin, K.Z., Li, G.M., Li, J.X., Yan, G., Su, D.K., Xiao, B., Chen, L., and Fan, X., 2009, Mineralization geochronology and geochemistry of Gangdise-Sharang molybdenum deposit and mineralization in the main period of Qinghai-Tibet Plateau collision: Acta Mineralogy Sinica, Supplement, 197–198.